

Quantum many-body scars in dual unitary circuits

Leonard Logarić,^{1,2,*} Shane Dooley,^{1,2,†} Silvia Pappalardi,³ and John Goold^{1,2,4}

¹*Department of Physics, Trinity College Dublin, Dublin 2, Ireland*

²*Trinity Quantum Alliance, Unit 16, Trinity Technology and Enterprise Centre, Pearse Street, Dublin 2, D02 YN67, Ireland*

³*Institut für Theoretische Physik, Universität zu Köln, Zùlpicher Straße 77, 50937 Köln, Germany*

⁴*Algorithmiq Ltd, Kanavakatu 3C 00160 Helsinki, Finland*

(Dated: July 14, 2023)

Dual-unitary circuits are a class of quantum systems for which exact calculations of various quantities are possible, even for circuits that are non-integrable. The array of known exact results paints a compelling picture of dual-unitary circuits as rapidly thermalising systems. However, in this work, we present a method to construct dual-unitary circuits for which some simple initial states fail to thermalise, despite the circuits being “maximally chaotic”, ergodic and mixing. This is achieved by embedding quantum many-body scars in a circuit of arbitrary size and local Hilbert space dimension. We support our analytic results with numerical simulations showing the stark contrast in the rate of entanglement growth from an initial scar state compared to non-scar initial states. Our results are well suited to an experimental test, due to the compatibility of the circuit layout with the native structure of current digital quantum simulators.

Introduction— Understanding how thermalisation arises in closed quantum systems is a fundamental problem in many-body physics. Currently, our best understanding is based on the eigenstate thermalisation hypothesis (ETH), which roughly states that thermalisation occurs because the individual eigenstates of the unitary propagator appear thermal with respect to local observables [1–5]. In this framework, failure to thermalise is due to the presence of non-thermal eigenstates. *Strong ergodicity breaking* occurs in systems where a significant fraction of all the eigenstates are non-thermal, while *weak ergodicity breaking* arises if only a negligibly small fraction of the eigenstates are non-thermal [6–9]. Strong ergodicity breaking is generally observed in systems with an extensive number of local conserved quantities, such as integrable [10] or many-body localised (MBL) systems [11, 12], while weak ergodicity can result in non-thermal eigenstates known as *quantum many-body scars* (QMBS) [6–9, 13–16].

Due to the complex nature of interacting many-body dynamics, exact results are notoriously hard to come by. Significant progress has been made in recent years, by studying a special class of toy models, called *dual unitary (DU) circuits*. These are a class of quantum circuits constructed as a brickwork pattern of two-qudit gates, which are unitary in both temporal and spatial directions. This special property enables the exact calculation of some system properties that would ordinarily be prohibitively hard to calculate [17–34].

For example, exact calculation of the spectral form factor has shown that interacting DU circuits are “maximally chaotic”, in the sense that the spectral form factor agrees with the predictions of random matrix theory at all timescales [18, 25]. Exact results also indicate that

DU circuits are fast scramblers of quantum information, since two-time correlation functions and out-of-time correlators (OTOCs) spread at their maximal possible velocities [19, 20]. In a similar spirit, from a certain class of solvable initial states it has been shown that entanglement growth occurs at the maximal rate [22, 24, 31] and that any finite subsystem thermalises to its maximally mixed (i.e., infinite temperature) reduced density matrix in a finite time [24]. Moreover, the exact results on two-time correlation functions allow a rigorous classification of DU circuits in terms of their ergodic and mixing properties [19, 28].

The above exact properties seem to indicate that generic DU circuits are rapidly thermalising systems [35]. This is further supported by the observation that it is impossible to induce MBL through disorder in DU circuits [18, 25], leaving integrability as the only known mechanism of strong ergodicity breaking in DU circuits. However, to be best of our knowledge, so far there has been no demonstration of weak ergodicity breaking in DU circuits, nor any arguments against it as in the case of MBL.

In this work, we show that weak ergodicity breaking is indeed possible in DU circuits. Using a projector-embedding approach, which was initially proposed for continuous time dynamics [36], we provide an explicit construction to insert QMBS in DU circuits of arbitrary system size and arbitrary local Hilbert space dimension. We demonstrate our construction with examples that embed a single, a few, or exponentially many QMBS in this class of circuits. Our construction shows that even provably “maximally chaotic”, ergodic and mixing systems can support QMBS. Despite the rapid scrambling properties of such systems, if the system is initialised in a QMBS all quantum information remains perfectly localised. Our analytical results are supported by numerical calculations for the entanglement growth, showing a striking difference in the dynamics between scar and non-scar initial states. Our work paves the way for future theoretical as well as experimental

* logaricl@tcd.ie

† dooleysh@gmail.com

investigations of weak ergodicity breaking in quantum circuits, where dual-unitarity can be leveraged [37, 38]. Due to the native structure of current digital quantum simulators, some of the proposed models can be adapted directly to current devices to probe their properties.

Dual Unitary Circuits– The basic building blocks of the circuits considered in this work are unitary operators, \hat{U} , acting on two qudits of arbitrary local Hilbert space dimension d . The *dual*, $\hat{\tilde{U}}$, of such a unitary is defined by a reordering of the subsystem indices [19]:

$$\langle k| \otimes \langle l|\hat{\tilde{U}}|i\rangle \otimes |j\rangle = \langle j| \otimes \langle l|\hat{U}|i\rangle \otimes |k\rangle, \quad (1)$$

and can be physically interpreted as an exchange of the spatial and temporal dimensions of the original gate. A gate \hat{U} is DU if and only if both \hat{U} and its dual $\hat{\tilde{U}}$ are unitary, $\hat{U}\hat{U}^\dagger = \hat{U}^\dagger\hat{U} = \hat{\tilde{U}}\hat{\tilde{U}}^\dagger = \hat{\tilde{U}}^\dagger\hat{\tilde{U}} = \hat{\mathbb{1}}$.

A complete parameterisation of DU gates is known for local Hilbert space dimension $d = 2$ [19], but has not been found yet for $d > 2$ [39]. However, any two-qudit gate of the form:

$$\hat{U}^{\text{DU},1} = (\hat{u}^+ \otimes \hat{u}^-) \hat{S} \hat{V} (\hat{v}^- \otimes \hat{v}^+), \quad (2)$$

is dual-unitary [39]. Here $\hat{S}|i\rangle \otimes |j\rangle = |j\rangle \otimes |i\rangle$ is the two-qudit swap operator, \hat{u}^\pm, \hat{v}^\pm are arbitrary single-qudit unitaries, and:

$$\hat{V} = \exp\left\{i \sum_{j=0}^{d-1} \hat{h}^{(j)} \otimes |j\rangle\langle j|\right\}, \quad (3)$$

is an entangling gate with arbitrary single-qudit Hermitian operators $\hat{h}^{(j)}$. We rewrite the non-entangling unitaries as:

$$\hat{u}^+ \otimes \hat{u}^- = \exp\{i(\hat{f}^+ \otimes \hat{\mathbb{1}} + \hat{\mathbb{1}} \otimes \hat{f}^-)\}, \quad (4)$$

$$\hat{v}^- \otimes \hat{v}^+ = \exp\{i(\hat{g}^- \otimes \hat{\mathbb{1}} + \hat{\mathbb{1}} \otimes \hat{g}^+)\}, \quad (5)$$

in terms of the single-qudit Hermitian operators \hat{f}^\pm and \hat{g}^\pm . With this parameterisation a dual-unitary gate is specified by the $d \times d$ Hermitian matrices $\hat{f}^\pm, \hat{g}^\pm, \hat{h}^{(j)}$. We also note that for any dual-unitary gate $\hat{U}^{\text{DU},1}$, the gate:

$$\hat{U}^{\text{DU},2} = \hat{S} \hat{U}^{\text{DU},1} \hat{S}^\dagger, \quad (6)$$

is also DU. Let us remark that generally this expression is not expressible in the form of Eq. (2), giving a distinct parameterisation of DU gates.

A DU circuit is a quantum circuit in a “brickwork” geometry, in which all of the individual two-qudit gates are DU. We consider an even number N of qudits, where each qudit has a local Hilbert space \mathbb{C}^d and the qudit sites are labelled by $n = 0, 1, 2, \dots, N-1$. We also assume periodic boundary conditions $n \equiv n+N$. The basic building blocks of the dynamics are local DU gates $\hat{U}_{n,n+1}$. A single timestep of the circuit

dynamics is implemented by a Floquet unitary operator $\hat{\mathbb{U}} = \hat{\mathbb{U}}_o \hat{\mathbb{U}}_e$ which is a layer of DU gates across even-odd bonds $\hat{\mathbb{U}}_e = \bigotimes_{j=0}^{N/2-1} \hat{U}_{2j,2j+1}$ and a layer of DU gates across odd-even bonds $\hat{\mathbb{U}}_o = \bigotimes_{j=1}^{N/2} \hat{U}_{2j-1,2j}$, forming the brickwork pattern. For simplicity, we will assume that all gates in the even layer are identical to each other and are in the form of Eq. (2), $\hat{U}_{0,1} = \hat{U}_{2,3} = \dots = \hat{U}^{\text{DU},1}$, and that all gates in the odd layer are identical to each other but swapped compared to the even layer unitaries, i.e., $\hat{U}_{1,2} = \hat{U}_{3,4} = \dots = \hat{U}^{\text{DU},2} = \hat{S} \hat{U}^{\text{DU},1} \hat{S}$. However, this two-site translation invariance is not essential for our results, which are also valid if the gates vary from site-to-site. Evolution for $t \in \mathbb{Z}$ timesteps is generated by powers of the Floquet operator $\hat{\mathbb{U}}^t$.

Embedding QMBS in DU circuits– In order to construct DU circuits with QMBS, we employ a projector embedding method, similar to the construction initially proposed by Shiraishi and Mori for continuous-time dynamics in Ref. [36]. The essential idea is to use projectors in the generators of the unitary gates in Eqs. (3), (4), (5), so that a chosen set of target states evolves by an elementary brickwork circuit of two-qudit swap gates, while states outside the target set evolve by a more complicated, possibly chaotic dynamics.

Let $\hat{P}_{n,n+1}$ denote two-qudit projectors acting on neighbouring sites n and $n+1$, and define the extended projectors acting on the total system of N qudits as:

$$\hat{\mathbb{P}}_{n,n+1} \equiv \hat{\mathbb{1}}_{0,n-1} \otimes \hat{P}_{n,n+1} \otimes \hat{\mathbb{1}}_{n+2,N-1}, \quad (7)$$

where $\hat{\mathbb{1}}_{i,j}$ is the identity acting on all qudits in the range $i, i+1, \dots, j-1, j$. The common kernel of all projectors is the set of states that are simultaneously annihilated by all of the $\hat{\mathbb{P}}_{n,n+1}$:

$$\mathcal{K} = \{|\psi\rangle : \hat{\mathbb{P}}_{n,n+1}|\psi\rangle = 0, \forall n\}. \quad (8)$$

Our target set of states \mathcal{T} , which we wish to embed in our circuit as QMBS, is the subset of \mathcal{K} that is invariant under the action of even and odd layers of swap gates:

$$\mathcal{T} = \{|\psi\rangle : |\psi\rangle \in \mathcal{K}, \hat{S}_e|\psi\rangle \in \mathcal{K}, \hat{S}_o|\psi\rangle \in \mathcal{K}\}, \quad (9)$$

where $\hat{S}_e = \bigotimes_{j=0}^{N/2-1} \hat{S}_{2j,2j+1}$ is the even layer of swap gates and $\hat{S}_o = \bigotimes_{j=1}^{N/2} \hat{S}_{2j-1,2j}$ is the odd layer.

We now outline a construction to embed this target space \mathcal{T} as a set of scars in our DU circuit. To do this we impose three conditions on the Hermitian generators $\{\hat{f}^\pm, \hat{g}^\pm, \hat{h}^{(j)}\}$ that define the DU gates in Eqs. (2)–(6):

$$\hat{P}_{n,n+1}(\hat{f}_n^+ \otimes \hat{\mathbb{1}} + \hat{\mathbb{1}} \otimes \hat{f}_{n+1}^-) \hat{P}_{n,n+1} = \hat{f}_n^+ \otimes \hat{\mathbb{1}} + \hat{\mathbb{1}} \otimes \hat{f}_{n+1}^-, \quad (C1)$$

$$\hat{P}_{n,n+1}(\hat{g}_n^- \otimes \hat{\mathbb{1}} + \hat{\mathbb{1}} \otimes \hat{g}_{n+1}^+) \hat{P}_{n,n+1} = \hat{g}_n^- \otimes \hat{\mathbb{1}} + \hat{\mathbb{1}} \otimes \hat{g}_{n+1}^+, \quad (C2)$$

$$\hat{P}_{n,n+1} \left(\sum_{j=0}^{d-1} \hat{h}_n^{(j)} \otimes |j\rangle\langle j|_{n+1} \right) \hat{P}_{n,n+1} = \sum_{j=0}^{d-1} \hat{h}_n^{(j)} \otimes |j\rangle\langle j|_{n+1}. \quad (C3)$$

Clearly two-qudit gates satisfying conditions (C1)–(C3) are still of the DU form in Eq. (2). Also, conditions (C1) and (C2) ensure that the single-qudit unitaries $\hat{u}_n^+ \otimes \hat{u}_{n+1}^-$ and $\hat{v}_n^+ \otimes \hat{v}_{n+1}^-$ act like the identity on all states in the common kernel \mathcal{K} of the projectors $\hat{P}_{n,n+1}$, while condition (C3) ensures that $\hat{V}_{n,n+1}$ acts like the identity on states in \mathcal{K} . However, even with conditions (C1)–(C3) the dynamics are not necessarily closed in the subspace \mathcal{K} . This is because the dual-unitary parameterisation of Eq. (2) also includes the swap operators $\hat{S}_{n,n+1}$ which can potentially take states out of \mathcal{K} . So, the QMBS subspace is the subspace $\mathcal{T} \subset \mathcal{K}$ that is invariant under even \hat{S}_e and odd \hat{S}_o layers of swap operators. For any initial state $|\psi\rangle \in \mathcal{T}$ the circuit will then act as $\hat{U}|\psi\rangle = \hat{S}|\psi\rangle$, where $\hat{S} = \hat{S}_o \hat{S}_e$, corresponding to integrable dynamics in the target subspace \mathcal{T} , even if the overall circuit \hat{U} is non-integrable and results in complicated dynamics for initial states that are not in \mathcal{T} . This prescription allows us to easily embed QMBS in the circuit and is the main result of this work. Since the circuit is DU by construction, all known exact results for DU circuits can be immediately imported and assumed for our DU circuit with QMBS.

Importantly, one of the key results on DU circuits is the rigorous classification in terms of their ergodic and mixing properties, based on the spectrum of a map \mathcal{M} which determines the dynamical correlation functions [19, 28]. We can show that our construction leads to QMBS in provably ergodic and mixing quantum many-body systems, since all dynamical correlation functions decay to their infinite temperature values at long times. Further details are provided in Appendix D.

Example A: single QMBS– We first illustrate our construction with the simplest possible example, for which the set of projectors is:

$$\hat{P}_{n,n+1} = \hat{\mathbb{I}}_{n,n+1} - |0\rangle\langle 0|_n \otimes |0\rangle\langle 0|_{n+1}, \quad (10)$$

for all $n = 0, 1, \dots, N-1$. The common kernel \mathcal{K} of all projectors consists of a single state $|0\rangle^{\otimes N}$, which is also invariant under the action of any product of swap gates so that the target space is the single state $\mathcal{T} = \{|0\rangle^{\otimes N}\}$. So, by our construction this state will be an eigenstate of the circuit $\hat{U}|0\rangle^{\otimes N} = |0\rangle^{\otimes N}$.

We choose the Hermitian generators $\{\hat{f}^\pm, \hat{g}^\pm, \hat{h}^{(j)}\}$ to be random, apart from some matrix rows/columns $\langle i|\hat{f}^\pm|0\rangle = \langle i|\hat{g}^\pm|0\rangle = \langle i|\hat{h}^{(0)}|0\rangle = 0$, $i \in \{0, 1, \dots, d-1\}$, that are set to zero to ensure that conditions (C1)–(C3) are satisfied. This choice gives a generic two-qudit DU gate which we expect to give a rapidly thermalising circuit. Moreover, we can prove that for this example our circuit is ergodic and mixing, as determined by the behaviour of its two-time correlation functions [19, 28] (see Appendix D).

Although this construction embeds QMBS for any system size N , we demonstrate our results with numerical simulations on finite size systems. In Fig. 1(a) we plot

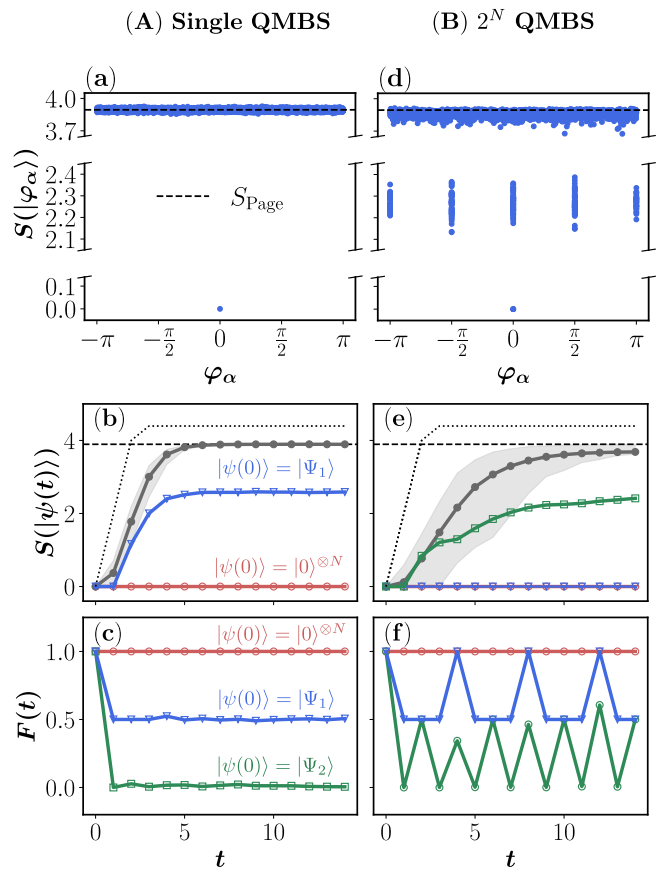


FIG. 1. Embedding a single QMBS (A) and an exponential number of QMBS (B) in a DU circuit. The top row (a,d) shows the bipartite entanglement of eigenstates $|\varphi_\alpha\rangle$ of the Floquet unitary \hat{U} in each case. The second row (b,e) shows the growth of bipartite entanglement, starting from different separable states. The grey line is the average entanglement growth for 100 random product states of the form $|\psi(0)\rangle = |i_0, i_1, \dots, i_{N-1}\rangle$, $i_n \in \{0, 1, \dots, d-1\}$, while the surrounding grey region shows the 5-95 percentile range. The dashed black line in (a, b, d, e) is the Page entropy, $S_{\text{Page}} = [N \ln(d) - 1]/2$. The dotted line in (b, d) shows the maximum possible rate of entanglement growth, saturating at the maximum value $S_{\text{max}} = N \ln(d)/2$. “Solvable” initial states have this maximal entanglement growth in the thermodynamic limit [22, 24, 40]. The bottom row (c,f) shows the overlap with the initial state $F(t) = |\langle \psi(0)|\psi(t)\rangle|$. The blue line in (b, c, e, f) shows the results for $|\Psi_1\rangle = |0\rangle^{N-1} \otimes [(|0\rangle + |d-1\rangle)/\sqrt{2}]$, and the green line for $|\Psi_2\rangle = |0, 0, d-1, d-1\rangle^{\otimes N/4-1} \otimes |0, 0, d-1\rangle \otimes (|d-1\rangle + |1\rangle)/\sqrt{2}$. [Parameters: $N = 8$, $d = 3$]

the half-system bipartite entanglement entropy:

$$S(|\varphi_\alpha\rangle) = -\text{Tr}[\hat{\rho}_\alpha \log(\hat{\rho}_\alpha)], \quad (11)$$

of the eigenstates $|\varphi_\alpha\rangle$ of the Floquet unitary \hat{U} . Here $\hat{\rho}_\alpha = \text{Tr}_{0, N/2-1} |\varphi_\alpha\rangle\langle \varphi_\alpha|$ is the reduced density matrix of the eigenstate obtained by tracing out the first $N/2$ qudits of the system. We clearly see the single QMBS $|0\rangle^{\otimes N}$ with zero entanglement, separated from the rest of the spectrum. All the other eigenstates are concentrated

around the Page entropy, S_{Page} , which is the expected value of entanglement entropy for a random pure state [41]. Further evidence of the QMBS can be seen in the dynamics. In Fig. 1(b) we show that, for the initial QMBS state $|\psi(0)\rangle = |0\rangle^{\otimes N}$, the bipartite entanglement $S(|\psi(t)\rangle)$ does not grow in time, and in Fig. 1(c) that the fidelity $F(t) = |\langle\psi(0)|\hat{U}^t|\psi(0)\rangle|$ remains constant at $F = 1$. By contrast, a typical random initial product state of the form $|\psi(0)\rangle = |\vec{i}\rangle \equiv |i_0, i_1, \dots, i_{N-1}\rangle$, with i_n chosen uniformly at random from the set $\{0, 1, \dots, d-1\}$, will give rapid growth in entanglement that saturates at the Page value S_{Page} , and will give a fidelity that decays rapidly to zero.

We further devise an initial state with intermediate slow dynamics. We consider the product state $|\psi(0)\rangle = |\Psi_1\rangle \equiv |0\rangle^{N-1} \otimes [(|0\rangle + |d-1\rangle)/\sqrt{2}]$. This initial state is partly overlapping with the QMBS $|0\rangle^{\otimes N}$ and is partly overlapping with the thermalising state $|0\rangle^{\otimes(N-1)} \otimes |d-1\rangle$. Correspondingly, the entanglement entropy saturates to a value intermediate between zero and the thermal value, while the fidelity approaches $F \approx 1/2$ after $t \sim 1$ timestep.

This construction can be extended to embed $k < d$ QMBS of the form $\{|\vec{i}\rangle^{\otimes N}\}_{i=0}^{k-1}$ into a DU circuit with local Hilbert space dimension d . The main adjustment is, instead of Eq. (10), to use the set of projectors $\hat{P}_{n,n+1} = \hat{\mathbb{I}}_{n,n+1} - \sum_{i=0}^{k-1} |i, i\rangle\langle i, i|_{n,n+1}$. We provide numerical demonstrations for the $k = 2$ case in Appendix C, as well as a discussion on how the circuit can be modified to break the eigenphase degeneracy between the QMBS in Appendix B.

Example B: Exponentially many QMBS—A more complex example is obtained by choosing the set of projectors:

$$\begin{aligned} \hat{P}_{n,n+1} = \hat{\mathbb{I}}_{n,n+1} & - |0\rangle\langle 0|_n \otimes |0\rangle\langle 0|_{n+1} \\ & - |0\rangle\langle d-1|_n \otimes |d-1\rangle\langle 0|_{n+1} \\ & - |d-1\rangle\langle 0|_n \otimes |0\rangle\langle d-1|_{n+1} \\ & - |d-1\rangle\langle d-1|_n \otimes |d-1\rangle\langle d-1|_{n+1}, \end{aligned} \quad (12)$$

for all n . Again, we choose the DU gate generators $\{\hat{f}^\pm, \hat{g}^\pm, \hat{h}^{(j)}\}$ to be random, apart from a few rows/columns that are set to zero to ensure that conditions (C1)–(C3) are satisfied [$\langle i|\hat{f}^\pm|j\rangle = \langle i|\hat{g}^\pm|j\rangle = \langle i|\hat{h}^{(j)}|j\rangle = 0$, $j \in \{0, d-1\}$, $i \in \{0, 1, \dots, d-1\}$].

The common kernel \mathcal{K} of the projectors in Eq. (12) is the 2^N -dimensional space spanned by the set of all N -qudit product states of the form $|\vec{i}\rangle = |i_0, i_1, \dots, i_{N-1}\rangle$ with $i_n \in \{0, d-1\}$. We note that this space, though exponentially large in the system size, is still an exponentially small fraction $(2/d)^N$ of the full Hilbert space, provided that $d > 2$. This space is also invariant under the action of both odd and even layers of swap gates $\hat{S}_{e/o}$ so that our target space is $\mathcal{T} = \mathcal{K}$. However, this does not mean that the product states $|\vec{i}\rangle$, $i_n \in \{0, d-1\}$, are QMBS since, in general, $\hat{U}|\vec{i}\rangle = \hat{S}|\vec{i}\rangle \neq |\vec{i}\rangle$. Instead, the

QMBS are found by diagonalising the swap circuit \hat{S} in the subspace spanned by $\{|\vec{i}\rangle\}_{i_n \in \{0, d-1\}}$.

In Fig. 1(d) we plot the eigenstate entanglement entropy of the eigenstates of \hat{U} . The bulk of the eigenstates have an entropy close to the Page value S_{Page} . However, the 2^N states in \mathcal{T} have a lower entanglement. There are, in fact, four QMBS that have zero entanglement. These are the states $|0\rangle^{\otimes N}$, $|d-1\rangle^{\otimes N}$, $|0, d-1\rangle^{\otimes N/2}$ and $|d-1, 0\rangle^{\otimes N/2}$ that are eigenstates of the swap circuit \hat{S} . The remaining $2^N - 4$ QMBS have non-zero entanglement, but are still clearly separated from the bulk of the spectrum which has a much larger entanglement close to the Page entropy.

The presence of exponentially many QMBS can also be observed in the dynamics, as shown from the entanglement entropy growth and fidelity dynamics in Fig. 1(e, f). When the system is initialized in a typical random product state (grey in the plot), it rapidly thermalizes to a highly entangled state. Conversely, for an initial product state in the QMBS subspace \mathcal{T} the entanglement growth is completely suppressed, since the swap circuit \hat{S} can only map product states to product states. For instance, the initial states $|\psi(0)\rangle = |0\rangle^{\otimes N}$ and $|\psi(0)\rangle = |\Psi_1\rangle \equiv |0\rangle^{N-1} \otimes (|0\rangle + |d-1\rangle)/\sqrt{2}$ [red and blue lines in Fig. 1(e)] show zero entanglement growth as they are both in the QMBS subspace \mathcal{T} .

However, the frozen entanglement from initial product states in \mathcal{T} does not capture all the information about the dynamics in the QMBS subspace, nor the variety of dynamical behaviours that are possible. For instance, evolution from $|\psi(0)\rangle = |\Psi_1\rangle = |0\rangle^{N-1} \otimes (|0\rangle + |d-1\rangle)/\sqrt{2}$ is characterised by an oscillating fidelity $F = |\langle\psi(0)|\psi(t)\rangle|$. This is due to the fact that $|\Psi_1\rangle$, although it is in the QMBS subspace, is a superposition of multiple QMBS. The $|0\rangle^{\otimes N}$ component of $|\Psi_1\rangle$ is a QMBS and does not decay, while the $|0\rangle^{\otimes(N-1)} \otimes |d-1\rangle$ component is a superposition of QMBS and leads to fidelity oscillations with a period $T = N/2$.

Alternatively, by initializing in $|\Psi_2\rangle = |0, 0, d-1, d-1\rangle^{\otimes N/4-1} \otimes |0, 0, d-1\rangle \otimes (|d-1\rangle + |1\rangle)/\sqrt{2}$ (green in Fig. 1) the system undergoes more rapid oscillatory dynamics. This initial state is an equal superposition of a state $|0, 0, d-1, d-1\rangle^{\otimes N/4}$ which is in the QMBS subspace and one that is not $|0, 0, d-1, d-1\rangle^{\otimes N/4-1} \otimes |0, 0, d-1, 1\rangle$. While the former leads to revivals in fidelity with period $T = 2$, the latter contribution rapidly decays to zero.

In Appendix D, we report further numerical results, including the dynamics of local observables, which provide further evidence for the generic rapid thermalisation of these models.

Discussion—Dual unitary circuits are a paradigmatic model for investigations in many-body phenomena due to the plethora of available exact results. In this work we have shown that these models can host QMBS, which lead to weak ergodicity breaking in a “maximally chaotic” system. We provide a systematic way to embed QMBS into DU circuits, and highlight the contrast with

the rest of the spectrum with numerical simulations.

The presented results motivate several fundamental questions, both with respect to DU circuits and chaotic quantum many-body systems in general. Due to the fact that the used parameterisations are not complete for a DU gates, we expect that there are many more DU circuit instances which can host QMBS. Furthermore, even for our parameterisation, our embedding approach is probably not exhaustive. Further investigations are required to obtain a more complete picture of QMBS in DU circuits and their properties.

The discovery of DU circuits was first motivated by the growing research of discrete time models, due to the architectures of current digital quantum simulators. However, research in recent years has shown that many quantities for these models can be calculated exactly. As such, they provide an invaluable benchmark for computations performed on current devices. The models presented in this work can be implemented on currently available hardware, demonstrating the existence of scars in discrete-time Floquet systems. Any deviations from

the expected exact results with respect to the fidelity revivals, entanglement growth, etc., can in turn be used as a benchmark for the quantum simulators.

ACKNOWLEDGMENTS

We acknowledge helpful conversations Jean-Yves Desaulles and Nathan Keenan. JG and LL acknowledge financial support by Microsoft Ireland. SD and JG acknowledge financial support from the SFI-EPSRC joint project QuamNESS. JG is supported by a SFI-Royal Society University Research Fellowship and acknowledges funding from European Research Council Starting Grant ODYSSEY (Grant Agreement No. 758403). S.P. acknowledges support by the Deutsche Forschungsgemeinschaft (DFG, German Research Foundation) under Germany's Excellence Strategy - Cluster of Excellence Matter and Light for Quantum Computing (ML4Q) EXC 2004/1 -390534769.

-
- [1] Luca D'Alessio, Yariv Kafri, Anatoli Polkovnikov, and Marcos Rigol, "From quantum chaos and eigenstate thermalization to statistical mechanics and thermodynamics," *Advances in Physics* **65**, 239–362 (2016).
- [2] Takashi Mori, Tatsuhiko N. Ikeda, Eriko Kaminishi, and Masahito Ueda, "Thermalization and prethermalization in isolated quantum systems: a theoretical overview," *Journal of Physics B: Atomic, Molecular and Optical Physics* **51**, 112001 (2018).
- [3] J. M. Deutsch, "Quantum statistical mechanics in a closed system," *Phys. Rev. A* **43**, 2046–2049 (1991).
- [4] Mark Srednicki, "Chaos and quantum thermalization," *Phys. Rev. E* **50**, 888–901 (1994).
- [5] Laura Foini and Jorge Kurchan, "Eigenstate thermalization hypothesis and out of time order correlators," *Physical Review E* **99**, 042139 (2019).
- [6] Maksym Serbyn, Dmitry A. Abanin, and Zlatko Papić, "Quantum many-body scars and weak breaking of ergodicity," *Nature Physics* **17**, 675–685 (2021).
- [7] Sanjay Moudgalya, B Andrei Bernevig, and Nicolas Regnault, "Quantum many-body scars and hilbert space fragmentation: a review of exact results," *Reports on Progress in Physics* **85**, 086501 (2022).
- [8] Zlatko Papić, "Weak ergodicity breaking through the lens of quantum entanglement," in *Entanglement in Spin Chains: From Theory to Quantum Technology Applications* (Springer, 2022) pp. 341–395.
- [9] Anushya Chandran, Thomas Iadecola, Vedika Khemani, and Roderich Moessner, "Quantum many-body scars: A quasiparticle perspective," *Annual Review of Condensed Matter Physics* **14**, 443–469 (2023).
- [10] Pasquale Calabrese, Fabian HL Essler, and Giuseppe Mussardo, "Introduction to 'quantum integrability in out of equilibrium systems'," *Journal of Statistical Mechanics: Theory and Experiment* **2016**, 064001 (2016).
- [11] Rahul Nandkishore and David A Huse, "Many-body localization and thermalization in quantum statistical mechanics," *Annu. Rev. Condens. Matter Phys.* **6**, 15–38 (2015).
- [12] Dmitry A. Abanin, Ehud Altman, Immanuel Bloch, and Maksym Serbyn, "Colloquium: Many-body localization, thermalization, and entanglement," *Rev. Mod. Phys.* **91**, 021001 (2019).
- [13] C. J. Turner, A. A. Michailidis, D. A. Abanin, M. Serbyn, and Z. Papić, "Weak ergodicity breaking from quantum many-body scars," *Nature Physics* **14**, 745–749 (2018).
- [14] Jean-Yves Desaulles, Francesca Pietracaprina, Zlatko Papić, John Goold, and Silvia Pappalardi, "Extensive multipartite entanglement from su(2) quantum many-body scars," *Phys. Rev. Lett.* **129**, 020601 (2022).
- [15] Shane Dooley, "Robust quantum sensing in strongly interacting systems with many-body scars," *PRX Quantum* **2**, 020330 (2021).
- [16] Shane Dooley, Silvia Pappalardi, and John Goold, "Entanglement enhanced metrology with quantum many-body scars," *Phys. Rev. B* **107**, 035123 (2023).
- [17] M Akila, D Waltner, B Gutkin, and T Guhr, "Particle-time duality in the kicked ising spin chain," *Journal of Physics A: Mathematical and Theoretical* **49**, 375101 (2016).
- [18] Bruno Bertini, Pavel Kos, and Tomaž Prosen, "Exact spectral form factor in a minimal model of many-body quantum chaos," *Phys. Rev. Lett.* **121**, 264101 (2018).
- [19] Bruno Bertini, Pavel Kos, and Tomaž Prosen, "Exact correlation functions for dual-unitary lattice models in 1 + 1 dimensions," *Phys. Rev. Lett.* **123**, 210601 (2019).
- [20] Pieter W. Claeys and Austen Lamacraft, "Maximum velocity quantum circuits," *Phys. Rev. Res.* **2**, 033032 (2020).
- [21] Sarang Gopalakrishnan and Austen Lamacraft, "Unitary circuits of finite depth and infinite width from quantum channels," *Phys. Rev. B* **100**, 064309 (2019).
- [22] Bruno Bertini, Pavel Kos, and Tomaž Prosen, "Entanglement spreading in a minimal model of maximal many-

- body quantum chaos,” *Phys. Rev. X* **9**, 021033 (2019).
- [23] Bruno Bertini and Lorenzo Piroli, “Scrambling in random unitary circuits: Exact results,” *Phys. Rev. B* **102**, 064305 (2020).
- [24] Lorenzo Piroli, Bruno Bertini, J. Ignacio Cirac, and Tomaž Prosen, “Exact dynamics in dual-unitary quantum circuits,” *Phys. Rev. B* **101**, 094304 (2020).
- [25] Bruno Bertini, Pavel Kos, and Tomaž Prosen, “Random matrix spectral form factor of dual-unitary quantum circuits,” *Communications in Mathematical Physics* **387**, 597–620 (2021).
- [26] S. Aravinda, Suhail Ahmad Rather, and Arul Lakshminarayanan, “From dual-unitary to quantum bernoulli circuits: Role of the entangling power in constructing a quantum ergodic hierarchy,” *Phys. Rev. Res.* **3**, 043034 (2021).
- [27] Felix Fritzsche and Tomaž Prosen, “Eigenstate thermalization in dual-unitary quantum circuits: Asymptotics of spectral functions,” *Phys. Rev. E* **103**, 062133 (2021).
- [28] Pieter W. Claeys and Austen Lamacraft, “Ergodic and nonergodic dual-unitary quantum circuits with arbitrary local hilbert space dimension,” *Phys. Rev. Lett.* **126**, 100603 (2021).
- [29] Alessio Lerose, Michael Sonner, and Dmitry A. Abanin, “Influence matrix approach to many-body floquet dynamics,” *Phys. Rev. X* **11**, 021040 (2021).
- [30] Cheryne Jonay, Vedika Khemani, and Matteo Ippoliti, “Triunitary quantum circuits,” *Phys. Rev. Res.* **3**, 043046 (2021).
- [31] Tianci Zhou and Aram W. Harrow, “Maximal entanglement velocity implies dual unitarity,” *Phys. Rev. B* **106**, L201104 (2022).
- [32] Ryotaro Suzuki, Kosuke Mitarai, and Keisuke Fujii, “Computational power of one-and two-dimensional dual-unitary quantum circuits,” *Quantum* **6**, 631 (2022).
- [33] Pieter W. Claeys, Marius Henry, Jamie Vicary, and Austen Lamacraft, “Exact dynamics in dual-unitary quantum circuits with projective measurements,” *Phys. Rev. Res.* **4**, 043212 (2022).
- [34] Márton Borsi and Balázs Pozsgay, “Construction and the ergodicity properties of dual unitary quantum circuits,” *Phys. Rev. B* **106**, 014302 (2022).
- [35] Hansveer Singh, Brayden A. Ware, Romain Vasseur, and Aaron J. Friedman, “Subdiffusion and many-body quantum chaos with kinetic constraints,” *Physical Review Letters* **127** (2021), 10.1103/physrevlett.127.230602.
- [36] Naoto Shiraishi and Takashi Mori, “Systematic construction of counterexamples to the eigenstate thermalization hypothesis,” *Phys. Rev. Lett.* **119**, 030601 (2017).
- [37] David T. Stephen, Wen Wei Ho, Tzu-Chieh Wei, Robert Raussendorf, and Ruben Verresen, “Universal measurement-based quantum computation in a one-dimensional architecture enabled by dual-unitary circuits,” (2022), [arXiv:2209.06191](https://arxiv.org/abs/2209.06191) [quant-ph].
- [38] Jesse C Hoke, Matteo Ippoliti, Dmitry Abanin, Rajeev Acharya, Markus Ansmann, Frank Arute, Kunal Arya, Abraham Asfaw, Juan Atalaya, Joseph C Bardin, *et al.*, “Quantum information phases in space-time: measurement-induced entanglement and teleportation on a noisy quantum processor,” [arXiv preprint arXiv:2303.04792](https://arxiv.org/abs/2303.04792) (2023).
- [39] Tomaž Prosen, “Many-body quantum chaos and dual-unitarity round-a-face,” *Chaos: An Interdisciplinary Journal of Nonlinear Science* **31**, 093101 (2021).
- [40] Alessandro Foligno and Bruno Bertini, “Growth of entanglement of generic states under dual-unitary dynamics,” *Physical Review B* **107** (2023), 10.1103/physrevb.107.174311.
- [41] Don N. Page, “Average entropy of a subsystem,” *Phys. Rev. Lett.* **71**, 1291–1294 (1993).
- [42] V.I. Arnold and A. Avez, *Ergodic Problems of Classical Mechanics*, Advanced book classics (Addison-Wesley, 1989).

Appendix A: Explicit construction

We here explicitly describe a construction of dual-unitary gates (defined by the $d \times d$ Hermitian matrices $\{\hat{f}^\pm, \hat{g}^\pm, \hat{h}^{(j)}\}$) satisfying conditions (C1)–(C3). We restrict our considerations to projectors of the form

$$\hat{P}_{n,n+1} = \hat{\mathbb{I}}_{n,n+1} - \sum_{x \in \mathcal{X}} |x\rangle\langle x|_{n,n+1}, \quad (\text{A1})$$

where \mathcal{X} is some set of orthonormal two-qudit states that we assume to be separable, i.e., $|x\rangle_{n,n+1} = |x'\rangle_n \otimes |x''\rangle_{n+1}$. For projectors of this form, conditions (C1) and (C2) can be satisfied by choosing the single-qudit Hermitian operators \hat{f}^\pm and \hat{g}^\pm such that $\hat{f}^+|x'\rangle = \hat{g}^-|x'\rangle = 0$ and $\hat{f}^-|x''\rangle = \hat{g}^+|x''\rangle = 0$, for all $|x\rangle = |x', x''\rangle \in \mathcal{X}$. This corresponds to setting some rows and columns of these matrices to zero. All of the other matrix elements can be chosen arbitrarily. It still remains to construct an entangling gate $\hat{V}_{n,n+1} = \exp\{\sum_{j=0}^{d-1} \hat{h}^{(j)} \otimes |j\rangle\langle j|\}$ that satisfies condition (C3). First, consider the two-qudit operator $\hat{H}_{n,n+1} = \sum_{j=0}^{d-1} \hat{h}'^{(j)} \otimes |j\rangle\langle j|$ where $\hat{h}'^{(j)}$ are arbitrary single-qudit Hermitian operators. This operator does not necessarily satisfy (C3). However, the projected operator $\hat{H}_{n,n+1} = \hat{P}_{n,n+1} \hat{H}_{n,n+1} \hat{P}_{n,n+1}$ is still of the form $\hat{H}_{n,n+1} = \sum_{j=0}^{d-1} \hat{h}^{(j)} \otimes |j\rangle\langle j|$ and is guaranteed to satisfy the condition (C3), since we have $\hat{P}_{n,n+1} \hat{H}_{n,n+1} \hat{P}_{n,n+1} = \hat{H}_{n,n+1}$.

In all of our numerical examples we construct a set of Hermitian generators $\{\hat{f}^\pm, \hat{g}^\pm, \hat{h}^{(j)}\}$ by first generating random matrices with elements $m_{j,k} = \alpha_{j,k} + i\beta_{j,k}$, where $\alpha_{j,k}, \beta_{j,k}$ are sampled from a uniform distribution. Random Hermitian matrices are then obtained as, e.g., $\hat{h} = \hat{m} + \hat{m}^\dagger$. Finally, we impose the conditions (C1), (C2), (C3) in the manner described above. This procedure is used in the following three examples:

- (A) $\mathcal{X} = \{|0, 0\rangle\}$, with the target space $\mathcal{T} = \{|0\rangle^{\otimes N}\}$ consisting of a single QMBS. The corresponding results can be found in **example A**, and in Fig. 1.
- (B) $\mathcal{X} = \{|0, 0\rangle, |d-1, d-1\rangle, |0, d-1\rangle, |d-1, 0\rangle\}$, in this case the target space is $\mathcal{T} = \text{span}\{|0\rangle, |d-1\rangle\}^{\otimes N}$, which has dimension $\dim(\mathcal{T}) = 2^N$. This gives an exponentially growing number of QMBS, though still an exponentially small fraction $(2/d)^N$ of all eigenstates for $d > 2$. The corresponding results can be found in **example B**, and in Fig. 1.
- (C) $\mathcal{X} = \{|0, 0\rangle, |d-1, d-1\rangle\}$, with the corresponding target space $\mathcal{T} = \text{span}\{|0\rangle^{\otimes N}, |d-1\rangle^{\otimes N}\}$, containing two QMBS. The results are presented in Appendix C.

Appendix B: Breaking QMBS eigenphase degeneracy

In examples with multiple QMBS it is possible that they can have a degeneracy in the eigenphase φ_α (where $\hat{U}|\varphi_\alpha\rangle = e^{i\varphi_\alpha}|\varphi_\alpha\rangle$). To determine the different possible values of the eigenphase for QMBS we observe that for QMBS we have $\hat{U}|\varphi_\alpha\rangle = \hat{S}|\varphi_\alpha\rangle = e^{i\varphi_\alpha}|\varphi_\alpha\rangle$ and that $\hat{S}^{N/2} = \hat{I}$. Hence:

$$\hat{S}^{N/2}|\varphi_\alpha\rangle = \exp\{iN\varphi_\alpha/2\}|\varphi_\alpha\rangle = |\varphi_\alpha\rangle \quad (\text{B1})$$

$$\implies e^{iN\varphi_\alpha/2} = 1 \quad (\text{B2})$$

$$\implies \varphi_\alpha = \frac{4\pi k}{N}, \quad (\text{B3})$$

where $k \in \{-\lfloor \frac{N}{4} \rfloor, -\lfloor \frac{N}{4} \rfloor + 1, \dots, \lfloor \frac{N}{4} \rfloor - 1\}$. Since there are only $N/2$ distinct values of the eigenphase and there must be degeneracies, for instance, in examples where we have an exponential number 2^N of QMBS.

However, some degeneracies in the QMBS in DU circuits can be broken by adding an additional unitary layer \hat{U}' at each timestep of the circuit with the properties $[\hat{S}, \hat{U}'] = 0$ and $[\hat{P}_{n,n+1}, \hat{U}'] = 0$ for all n . These properties ensure that the projectors and the swap layers share a set of simultaneous eigenstates with \hat{U}' , including the QMBS in \mathcal{K} . If \hat{U}' can be constructed as a product of one-qudit gates then these gates can be absorbed into the even or odd layer unitaries $\hat{U}_{e/o}$ without disturbing the brickwork structure of the circuit and without impacting dual unitarity. This approach to break the QMBS eigenphase degeneracy is the example in Appendix C below, where we embed two QMBS in a DU circuit.

Appendix C: An example with two QMBS

In order to embed two QMBS into a DU circuit, we choose the following set of projectors:

$$\hat{P}_{n,n+1} = \hat{I}_{n,n+1} - |0\rangle\langle 0|_n \otimes |0\rangle\langle 0|_{n+1} - |d-1\rangle\langle d-1|_n \otimes |d-1\rangle\langle d-1|_{n+1}, \quad (\text{C1})$$

which will lead to the common kernel $\mathcal{K} = \{|0\rangle^{\otimes N}, |d-1\rangle^{\otimes N}\}$. Since any state of the form $|i\rangle^{\otimes N}$ is invariant under the application of a layer of swap gates $\hat{S}_{e/o}$, the target space will be the same as the kernel, $\mathcal{T} = \mathcal{K}$. In order to construct the DU gate generators $\{\hat{f}^\pm, \hat{g}^\pm, \hat{h}^{(j)}\}$ we follow the procedure described in A, guaranteeing that they will obey the required conditions (C1), (C2), (C3). Once the generators are constructed, we numerically calculate the same quantities as for examples A and B in the main text. The result is a circuit with the two QMBS $\hat{U}|0\rangle^{\otimes N} = |0\rangle^{\otimes N}$ and $\hat{U}|d-1\rangle^{\otimes N} = |d-1\rangle^{\otimes N}$ that have the same eigenphase $|\varphi\rangle = 0$.

However, we also break the QMBS eigenphase degeneracy by adding an additional layer of single qudit unitaries $\hat{U} \rightarrow \hat{U}\hat{U}'$, where $\hat{U}' = \hat{u}_\phi^{\otimes N}$ and $\hat{u}_\phi = \sum_{j=0}^{d-1} \exp\{-i\phi \frac{2j-(d-1)}{d-1}\} |j\rangle\langle j|$ are generalised Pauli Z-rotations (see Appendix B above). This additional layer of single-qudit unitaries will add a phase of $e^{iN\phi}$ to the $|0\rangle^{\otimes N}$ state, whereas the other QMBS state, $|d-1\rangle^{\otimes N}$, will acquire an eigenphase of $e^{-iN\phi}$. In the performed computations we set $\phi = 0.01$.

The numerical results are shown in Fig. 2. The entanglement growth (Fig 2 - centre) and fidelity evolution (Fig. 2 - right) are quantitatively very close to the ones obtained for the single QMBS case (1 - b, c). The only major difference can be observed in the plot of entanglement entropies and eigenphases of the individual eigenstates (Fig. 2 - left), where we now observe two QMBS at 0 entanglement entropies, both having a non-zero eigenphases due to the choice of phase degeneracy breaking single-qudit unitaries. .

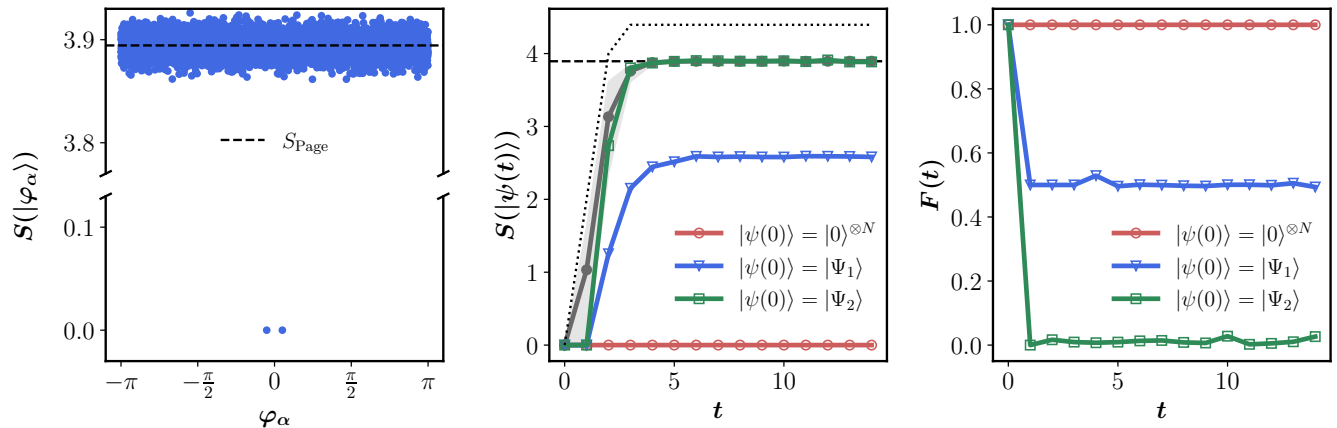


FIG. 2. An example illustrating out construction with two QMBS. (Left) The entanglement entropy and eigenphases of individual eigenstates of the Floquet operator. Most of the spectrum has an entanglement entropy close to the Page value, while the QMBS states, $\{|0\rangle^{\otimes N}, |d-1\rangle^{\otimes N}\}$ are at 0 entanglement entropy and have non-zero phases, due to the chosen single-qudit unitaries. (Centre) Entanglement entropy growth for the set of initial states as used in a two-qudit unitary in Fig. 1, and we observe quantitatively similar results as in example A. (Right) Time evolution of fidelity with respect to the initial state. [Parameters: $N = 8$, $d = 3$]

Appendix D: Ergodic Properties of Presented Models

The ergodic properties of a quantum many-body system can be characterized by the behaviour of its dynamical correlation functions [42]. For DU circuits, in particular, it has been shown that the dynamical correlation functions can be calculated exactly [19], and are directly related to the spectral properties of a completely-positive and trace-preserving map \mathcal{M}_ν , where $\nu = \pm$ denotes the direction along which we are computing the correlation function. For our circuit setup, with DU gates \hat{U}_e^{DU} making up the even layer and DU gates \hat{U}_o^{DU} making up the odd layer, the map can be written as $\mathcal{M}_\nu = \mathcal{M}_{\nu,o}\mathcal{M}_{\nu,e}$, with:

$$\mathcal{M}_{+,e/o}(\hat{o}) \equiv \frac{1}{d} \text{Tr}_1[(\hat{U}_{e/o}^{\text{DU}})^\dagger (\hat{o} \otimes \hat{\mathbb{I}}) \hat{U}_{e/o}^{\text{DU}}], \quad (\text{D1})$$

$$\mathcal{M}_{-,e/o}(\hat{o}) \equiv \frac{1}{d} \text{Tr}_2[(\hat{U}_{e/o}^{\text{DU}})^\dagger (\hat{\mathbb{I}} \otimes \hat{o}) \hat{U}_{e/o}^{\text{DU}}], \quad (\text{D2})$$

where \hat{o} is an arbitrary local observable and $\text{Tr}_{1/2}$ is a partial trace over the left/right qudit [27].

The mathematical properties of \mathcal{M}_ν guarantee that all of its eigenvalues lie on or within a unit circle, centered at the origin of the complex plane. The single qudit identity operator $\hat{o} = \hat{\mathbb{I}}$ is always an eigenoperator of \mathcal{M}_ν with unit eigenvalue, i.e., $\mathcal{M}_\pm(\hat{\mathbb{I}}) = \hat{\mathbb{I}}$. If there is one or more additional eigenoperators of \mathcal{M}_\pm with unit eigenvalue then the circuit is *non-ergodic*, since these additional eigenoperators correspond to non-decaying dynamical correlation functions. On the other hand, if the single-qudit identity operator is the only eigenvector of \mathcal{M}_\pm with unit eigenvalue then the circuit is *ergodic* and all time-averaged dynamical correlation functions approach their thermal values at large times. If, in addition, there are no other eigenvalues of \mathcal{M}_\pm with unit modulus, then the circuit is also *mixing*.

For the DU circuit setup in this work we have chosen the even layer DU gates to be of the form $\hat{U}_e^{\text{DU}} = \hat{U}^{\text{DU},1}$ (c.f. Eq. 2) and the odd layer DU gates to be of the form $\hat{U}_o^{\text{DU}} = \hat{U}^{\text{DU},2}$ (c.f. Eq. 6). With this choice we obtain a map \mathcal{M}_\pm that has a single eigenvalue with unit modulus, corresponding to the identity eigenoperator, and therefore the DU circuit will display ergodic and mixing behaviour according to the classification described above. This is shown numerically in Fig. 3 where we plot the eigenvalues λ_\pm of \mathcal{M}_\pm for each of our three examples (example A and example B in the main text, as well as the two QMBS example in Appendix C). [We have observed that the circuit is also ergodic and mixing if we choose $\hat{U}_e^{\text{DU}} = \hat{U}^{\text{DU},2}$ and $\hat{U}_o^{\text{DU}} = \hat{U}^{\text{DU},1}$.]

However, it is also possible to embed QMBS in DU circuits that are *non-ergodic*. This can be achieved by choosing even and odd layer gates to be the same [i.e., $\hat{U}_e^{\text{DU}} = \hat{U}_o^{\text{DU}} = \hat{U}^{\text{DU},1}$ or $\hat{U}_e^{\text{DU}} = \hat{U}_o^{\text{DU}} = \hat{U}^{\text{DU},2}$]. In this case the \mathcal{M}_\pm maps will have 2 eigenvalues with unit modulus, and thus the DU circuit will be non-ergodic by the classification described above.

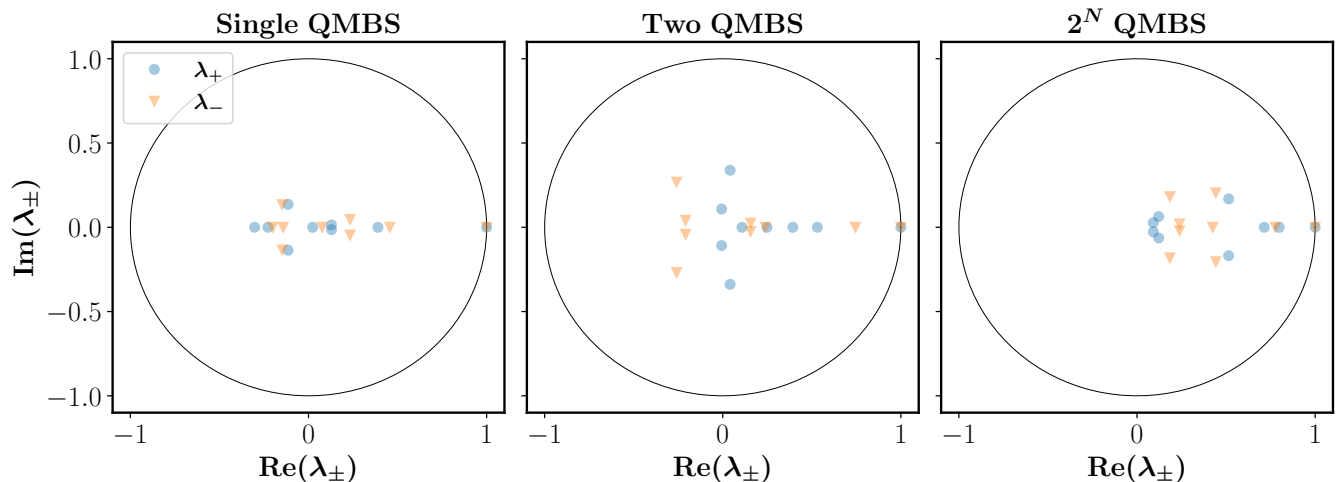


FIG. 3. Eigenvalues of the \mathcal{M}_\pm map for the three models presented in this work. For all of the models we can observe exactly one eigenvalue of $\lambda_\pm = 1.0$, corresponding to the identity operator $\hat{o} = \hat{\mathbb{1}}$. All of the other eigenvalues of \mathcal{M}_\pm satisfy $|\lambda_\pm| < 1$, thus demonstrating that the presented models fall within the ergodic and mixing class according to the classification presented in [19].

Appendix E: ETH and dynamics of local observables

By the eigenstate thermalisation hypothesis (ETH) we expect thermalising systems to have eigenstate expectation values that are close to the thermal expectation values (for local observables). If all eigenstates are thermal then the corresponding observables will thermalise, starting from a non-equilibrium state. However, non-thermal eigenstates, like QMBS can prevent thermalisation. In our circuit model, since energy is not conserved, the thermal expectation values are with respect to the infinite temperature state $\hat{\rho}_{T=\infty} = \hat{\mathbb{1}}/d^N$.

We check these features in our DU circuit with QMBS for the local observable

$$\hat{S}_{\text{tot}}^z = \sum_{n=0}^{N-1} \hat{S}_n^z, \quad \hat{S}_n^z = \sum_{i=0}^{d-1} \frac{2i - (d-1)}{d-1} |i\rangle\langle i|_n, \quad (\text{E1})$$

where \hat{S}_n^z is the local magnetisation at site n . In Fig. 4, top row, we can clearly see that the QMBS in the three example models are well separated from the rest of the spectrum, which is concentrated around $S_{\text{tot}}^z \approx 0$, the expectation value for the infinite temperature thermal state. These QMBS can prevent thermalisation of the total magnetisation \hat{S}_{tot}^z . To show this, we also numerically calculate the dynamics of the expectation value of \hat{S}_{tot}^z/N for the set of initial states that were previously used to probe entanglement growth and fidelity evolution.

As expected, the $|0\rangle^{\otimes N}$ state, which is a QMBS in all three models, gives a failure to thermalise in any of the examples.

The $|\Psi_1\rangle = |0\rangle^{\otimes N-1} \otimes (|0\rangle + |d-1\rangle)/\sqrt{2}$ state is an equal superposition of the QMBS $|0\rangle^{\otimes N}$, and the state $|0\rangle^{\otimes N-1}|d-1\rangle$ which is in the QMBS subspace only for the model with exponentially many QMBS. Hence, for the single- and two-QMBS examples we observe the magnetisation density approaching $\langle \hat{S}_{\text{tot}}^z \rangle / N \approx -0.5$ (since the non-QMBS component thermalises but the QMBS component does not). In the model with exponentially many QMBS, the state $|\Psi_1\rangle$ is in the QMBS subspace. Although the state evolves in a non-trivial way [see Fig. 1(f) in the main text] the dynamics by the swap circuit \hat{S} preserves the total magnetization, as shown in the blue line in the bottom right plot of Fig. 4.

The $|\Psi_2\rangle = |0, 0, d-1, d-1\rangle^{\otimes N/4-1} \otimes |0, 0, d-1\rangle \otimes (|d-1\rangle + |1\rangle)/\sqrt{2}$ initial state has an expectation value of $\langle \hat{S}_{\text{tot}}^z \rangle / N = 0$ for the total magnetisation, but is not in the QMBS subspace for the single- and two-QMBS examples. Therefore we initially see some oscillations at early times, with the expectation value approaching the thermal one for $t \sim \mathcal{O}(10)$. However, for the exponential QMBS example, the initial state $|\Psi_2\rangle$ is entirely in the QMBS subspace, and therefore undergoes dynamics by the swap circuit \hat{S} which conserves the total magnetization.

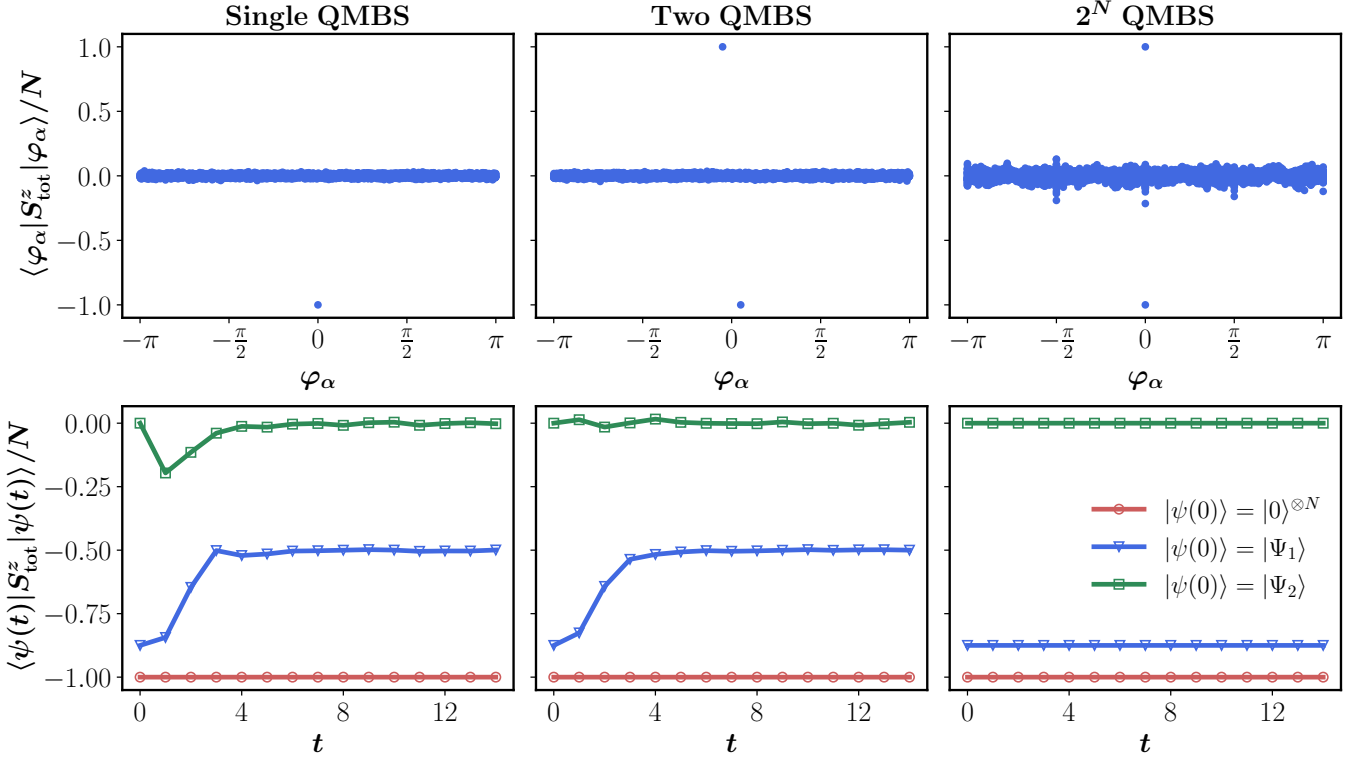


FIG. 4. QMBS in DU circuits, shown through the observable $\hat{S}_{\text{tot}}^z = \sum_{n=0}^{N-1} \hat{S}_n^z$, where $\hat{S}_n^z = \sum_{i=0}^{d-1} (2i - d) |i\rangle\langle i|_n$ is the local magnetization at site n . Top row: the expectation values of eigenstates of the Floquet operator \hat{U} for the observable \hat{S}_{tot}^z/N . Most eigenstates are concentrated around the infinite-temperature thermal value $\langle \hat{S}_{\text{tot}}^z \rangle_{\text{th}} = \text{Tr}[\hat{S}_{\text{tot}}^z \hat{\Pi}]/d^N = 0$, though QMBS are clearly visible in our three examples. Bottom row: dynamics of the expectation value of the total magnetization, starting from different separable states. The initial state $|\psi(0)\rangle = |0\rangle^{\otimes N}$ (red line) is a QMBS in each example, and therefore gives no change in the total magnetization \hat{S}_{tot}^z . Other initial states are $|\Psi_1\rangle = |0\rangle^{\otimes N-1} \otimes (|0\rangle + |d-1\rangle)/\sqrt{2}$ (blue) and $|\Psi_2\rangle = |0, 0, d-1, d-1\rangle^{\otimes N/4-1} \otimes |0, 0, d-1\rangle \otimes (|d-1\rangle + |1\rangle)/\sqrt{2}$ green. [Parameters: $N = 8$, $d = 3$]